



Influence of the specimen geometry on *R*-curve behavior and roughening of fracture surfaces

STÉPHANE MOREL¹, GUILLAUME MOUROT^{1,2} and JEAN SCHMITTBUHL³

¹Lab. de Rhéologie du Bois de Bordeaux, UMR 5103, Domaine de l'Hermitage, 69 route d'Arcachon, 33612 Cestas Cedex, France

²C.E.A. Saclay, (D.S.M./D.R.E.C.A.M./S.P.C.S.I.), 91191 Gif-Sur-Yvette Cedex, France

³Lab. de Géologie, UMR 8538, Ecole Normale Supérieure, 24 rue Lhomond, 75231 Paris Cedex 05, France

Abstract. Recently the *R*-curve behavior observed on quasi-brittle materials was proposed to be related to the roughness development of fracture surfaces. However, many experiments have shown that the *R*-curve behavior is not a material property but depends on the specimen shape. It is also expected that the roughening of fracture surfaces is influenced by the specimen geometry and so *R*-curve behaviors related to this roughening. From mode I fracture tests on wood specimens of three different shapes, *R*-curves are estimated and the morphology of the crack surfaces are analysed. We show that the scaling exponents of the *anomalous* scaling law used to describe accurately the roughness development of crack surfaces, are not influenced by the specimen geometry and appear as material dependent parameters. Nevertheless, the fracture surfaces exhibit a roughness growth region that reduces with the *average* stiffness of the specimens. Accordingly, the maximum roughness magnitude of fracture surfaces is a function of the initial stiffness: the higher the stiffness, the smaller the maximum magnitude of the roughness. We show that the analytical *R*-curves deduced from the roughening of fracture surfaces provide good fits of the experimental macroscopic *R*-curves. However, if the scaling exponents obtained from the *R*-curve fits are close to those measured from the microscopic roughness analysis, the description of the experimental *R*-curves requires a magnification of the real area of the main crack. This magnification can be explained by the weakness of the assumption of an energy only dissipated by a single crack and not by a process zone. Finally, we argue that an approach where the energy is dissipated by a set of microcracks that follow the same *anomalous* scaling, could fully explain the experimental *R*-curves.

Key words: Quasibrittle materials, specimen geometry, *R*-curve, roughening, fractal cracks, microcracking.

1. Introduction

Since the early work of Mandelbrot et al. (1984), the study of the morphology of fracture surfaces is nowadays a very active field of research. Observations have shown that, the fracture surfaces for different materials are statistically very well described by self-affine fractals (see e.g., Bouchaud, 1997). However, studies of the complete roughness development of fracture surfaces obtained in quasi-brittle materials like granite or wood (Schmittbuhl et al., 1994; López and Schmittbuhl, 1998; Morel et al., 1998), have shown the anisotropy of the crack developments between the crack propagation direction and the direction transverse to it. Moreover it has been shown that roughness grows in two steps: a fast and a slow step. The latter leads to an important implication. The magnitude of the roughness far from the initiation notch, is a function of the sample size at any scales (i.e. even at scales significantly smaller than the sample). An accurate description of this growth is provided by a particular scaling law, called *anomalous* scaling (López and Rodríguez, 1996), which implies the existence of

three scaling exponents instead of the single Hurst exponent (or local roughness exponent ζ_{loc}) generally used. The two additional scaling exponents, named global roughness exponent ζ and dynamic exponent z , have been shown as material dependent parameters (López and Schmittbuhl, 1998; Morel et al., 1998) unlike the local roughness exponent ζ_{loc} which the very robust value has been experimentally demonstrated in the past (Bouchaud et al., 1990; Bouchaud, 1997) and recently explained theoretically (Hansen and Schmittbuhl, 2003; Schmittbuhl et al., 2003).

As a mechanical point of view, the roughness of the fracture surfaces subsequently increase the effective fracture energy of materials and hence, may be considered as a potential source of toughening. Thus, in the last few years, many attempts were made to establish connections between the fracture energy (or toughness) of materials and either the fractal dimension (Mosolov, 1993; Carpinteri, 1994; Balankin, 1996; Borodich, 1997; Bažant, 1997; Weiss, 2001b) or to relevant lengthscales (Bouchaud and Bouchaud, 1994). Nevertheless, almost all these connections were established on the basis of a crack surface only characterized by its fractal dimension (which is related to the local roughness exponent ζ_{loc} : $d_F = 3 - \zeta_{loc}$) and do not take into account the growth of the cracks such as the one observed in the quasi-brittle materials. The anomalous roughening of quasi-brittle materials was recently proposed to be related to the macroscopic elastic energy released during crack propagation (Morel et al., 2000). This connection between roughening of crack surfaces and material fracture properties yields more accurate estimates of the resistance curve behavior (Morel et al., 2000b) and of the size effect (Morel et al., 2000a), which are generally characteristic of the fracture behavior of quasi-brittle materials.

The dependence of the predicted R -curve on the material has been established from the observation that the global roughness and dynamic exponents (respectively ζ and z) are material dependent parameters (Morel et al., 1998). However the eventual dependence on the specimen geometry is not yet established. Otherwise, many experiments have shown that the R -curve behavior observed in quasi-brittle materials should not be considered as a material property since they exhibit strong dependence on the specimen geometry (see e.g., Bažant and Kazemi, 1990). Accordingly the R -curve, deduced from the connection between fractal nature of cracks and material fracture properties, is expected to be geometry dependent.

In this paper, we focus on the link between the specimen shape and the R -curve behavior by means of the roughness description in terms of anomalous scaling. The experimental setup for mode I fracture tests made on wood specimens of three different shapes (derived from the double cantilever beam specimen), is described in Section 2. From load-deflection values, the energy release rates are estimated as a function of the crack length increment and R -curve behaviors for three specimen geometries are observed. In Section 3, a roughness analysis of numerous fracture surfaces is performed. We show that the *anomalous* scaling law provides an accurate description of the roughness development of crack surfaces. The scaling exponents obtained from this description are shown not to be influenced by the specimen geometry and so are material dependent parameters. Nevertheless, the extension of the roughness growth regions is shown to be dependent on the specimen shape. As a consequence, the magnitude of the sample roughness is a function of its shape. From the accurate description of the roughness development of crack surfaces, we show in Section 4 that good fits of the macroscopic resistance curves are obtained on the basis of the predicted R -curves deduced from the microscopic description of the fracture roughness. However the fit leads to a magnification of the cracked areas compared to those estimated directly from the roughness analysis. The implications of such a magnification of cracked surfaces for fracture process are discussed in Section 4.3.

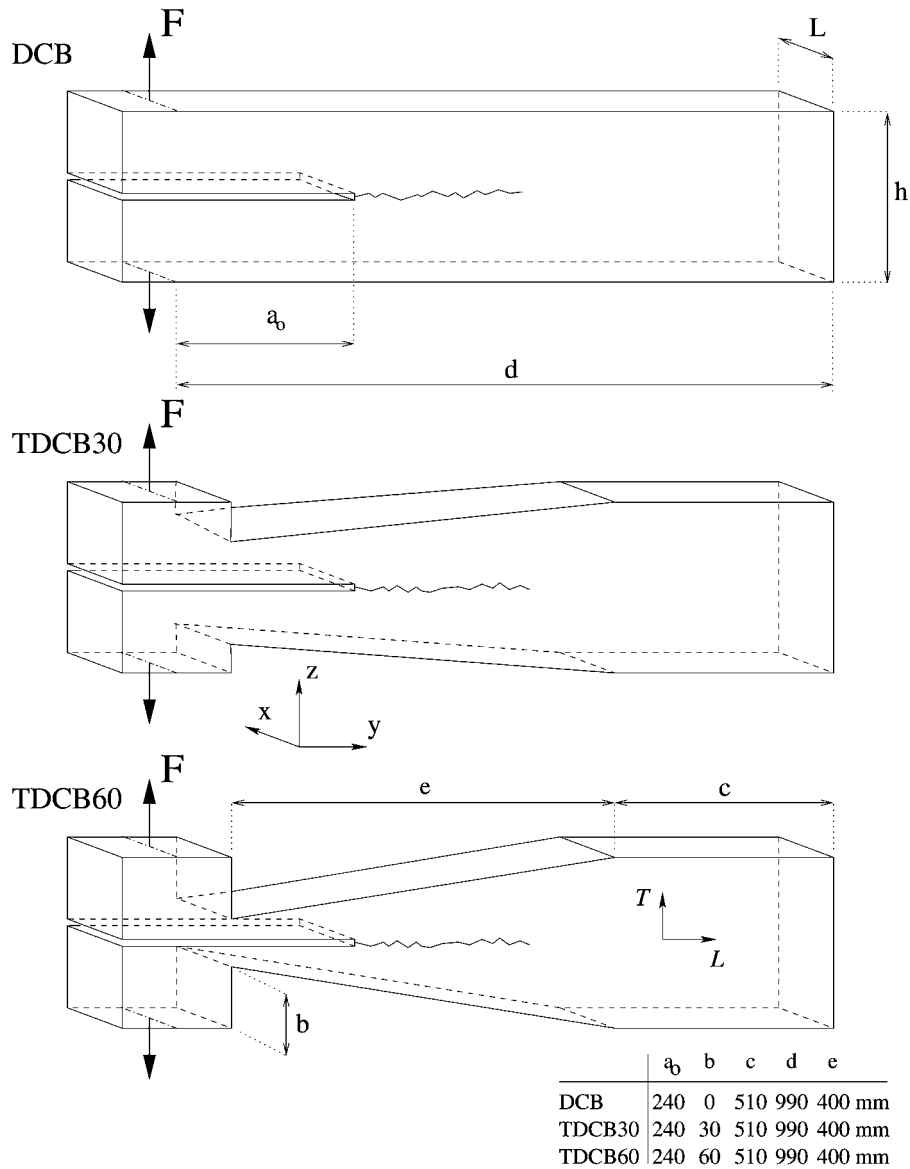


Figure 1. Mode I fracture specimens of three different shapes: a double cantilever beam specimen (DCB) and two sorts of tapered double cantilever beam specimens (respectively TDCB30 and TDCB60).

2. Experiment

In the following the experimental setup of fracture tests in mode I wood specimens of three different shapes is described. The tested wood species is a Spruce (*Picea excelsa* W.). The average oven dry specific density was 0.42 and the moisture content of all tested specimens was measured between 13% and 15%. The tests were made on three kinds of mode I fracture specimens of 1 m long: a double cantilever beam specimen (denoted DCB) and two sorts of modified tapered double cantilever beam specimens (respectively denoted TDCB30 and TDCB60) (see Fig. 1). The depth b of the lateral notches of the two TDCB specimens is 30 or 60 mm and all dimensions of the specimens are reported in Fig. 2. On the three kinds of

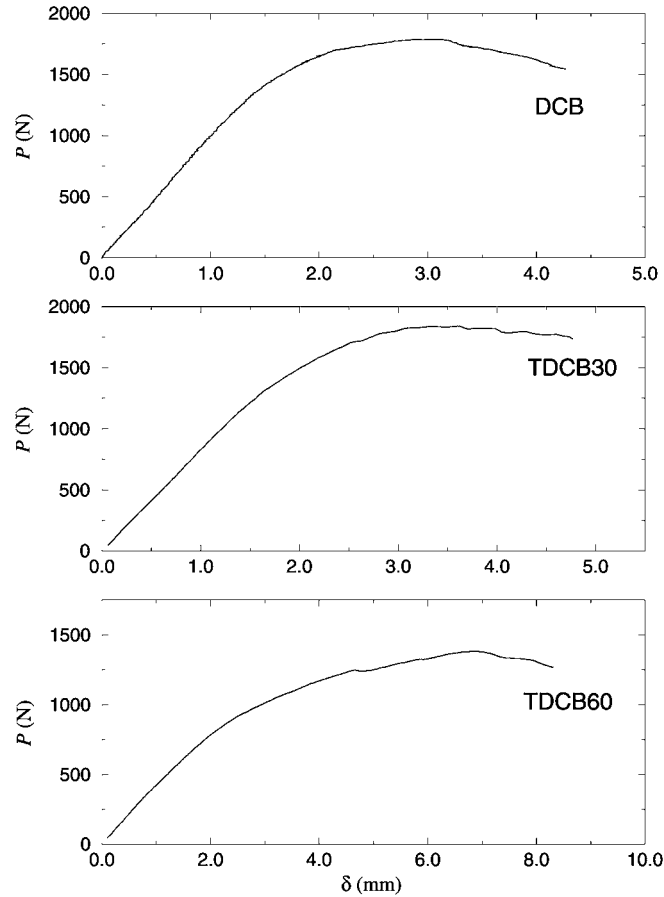


Figure 2. Typical load-deflection values obtained from the three specimen shapes.

fracture specimens an initial straight notch is machined with a band saw (thickness 2 mm) and extended over a few millimeters with a razor blade (thickness 0.2 mm). The fracture is obtained through an uniaxial tension at a constant opening rate. The average crack plane corresponds to the radial-longitudinal plane of wood, the longitudinal direction is the direction of crack propagation. During the tests, load-deflection values were continuously recorded and typical curves obtained for each sort of fracture specimens are plotted in Fig. 2.

It is now well established that the fracture of quasi-brittle material such as wood can be described through an equivalent linear elastic problem (Bažant and Kazemi, 1990; Bažant, 1997; Morel et al., 2002b) where the increase of specimen compliance is translated in terms of an elastically equivalent crack propagation.

The dependence of the compliance of our samples on the crack length increment has been computed using a finite element method for the three specimen shapes and with the elastic characteristics of wood. On this basis, the elastic energy release rates G_R are estimated from the load-deflection curves for any crack length increment Δa (defined as: $\Delta a = a - a_o$ where a is the elastically equivalent length of the crack and a_o is the length of the initial notch). For a given crack length increment Δa , the energy release rate G_R is computed from the elastic energy released during a small crack propagation δa (corresponding to the filled area on Fig. 3). Figure 4 shows the evolution of the energy release rate G_R as a function of the

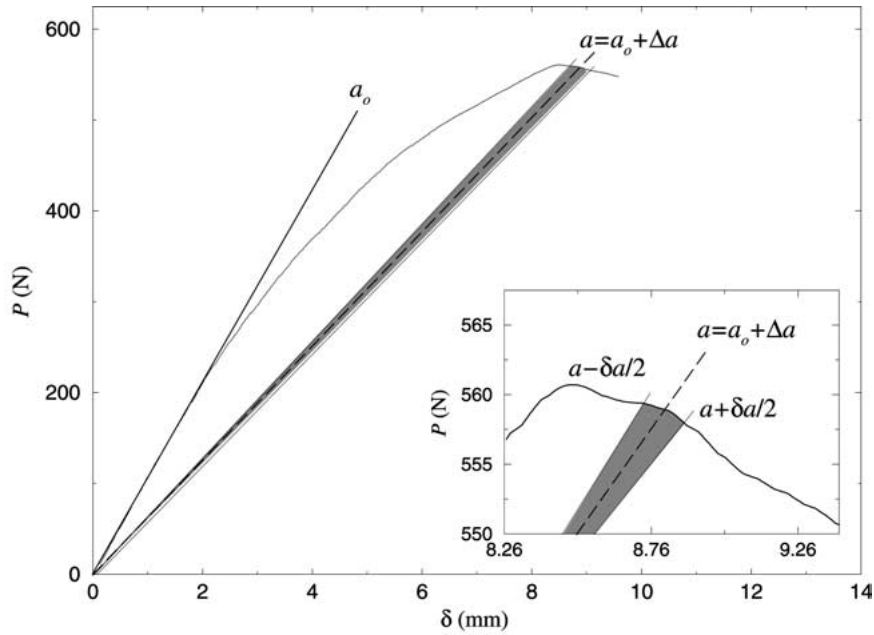


Figure 3. Method for the determination of the elastic energy release rate $G_R = A/(\delta a L)$ where A is the filled area corresponding to the elastic energy released during a small crack extension δa ($\delta a = 0.3$ mm).

crack length increment Δa obtained for the three kinds of specimen. Pronounced R -curves are observed, i.e., an evolution of the resistance to crack growth with the crack length increment Δa (Lawn, 1993). The R -curve behavior is followed after a characteristic crack advance Δa_c , by a propagation at constant resistance to crack growth. The transition defines a *critical* value of the resistance denoted $G_{RC} = G_R(\Delta a_c)$ that arises approximately at the peak load of the specimens. Note that, as shown in Table 1, the critical resistance G_{RC} and the crack length increment Δa_c are dependent on the *average* compliance of the specimens (which increases with the depth b of the lateral notches, Fig. 1). This can be explained by a strong difference of the stress intensity factors as a function of the specimen geometry. Indeed in Fig. 5, the dimensionless stress intensity factor function $k(\Delta a)$ obtained from a finite element method is plotted with respect to the crack length increment Δa for the three shapes of specimen. Thus, from Fig. 5, the stress intensity factor K obtained for a unity load P and for various crack length increments Δa (lower than 200 mm), is respectively greater for TDCB60 than for TDCB30 and DCB. Hence, for the same crack advance Δa and under the same load, the fracture process zone is expected to be larger for TDCB60 specimen rather than for TDCB30 or DCB specimens. Accordingly the R -curve behavior (which corresponds to the release of stored energy engendered by the process zone) is expected to last for larger crack length increments Δa_c and will correspond to higher critical resistance to crack growth G_{RC} for TDCB60 rather than TDCB30 or DCB specimens.

Topographies of crack surfaces were also recorded using an optical profiler (double triangulation laser sensor) along regular grids oriented along the x direction, that is parallel to the initial notch and along the radial direction of wood. The y direction is the direction of crack propagation and corresponds to the longitudinal direction of wood. Each map was built with up to 100 profiles of 2050 points along the x direction. The step of sampling in the x direction was adjust to the cell width ($\Delta x = 25 \mu\text{m}$) while the distance between two

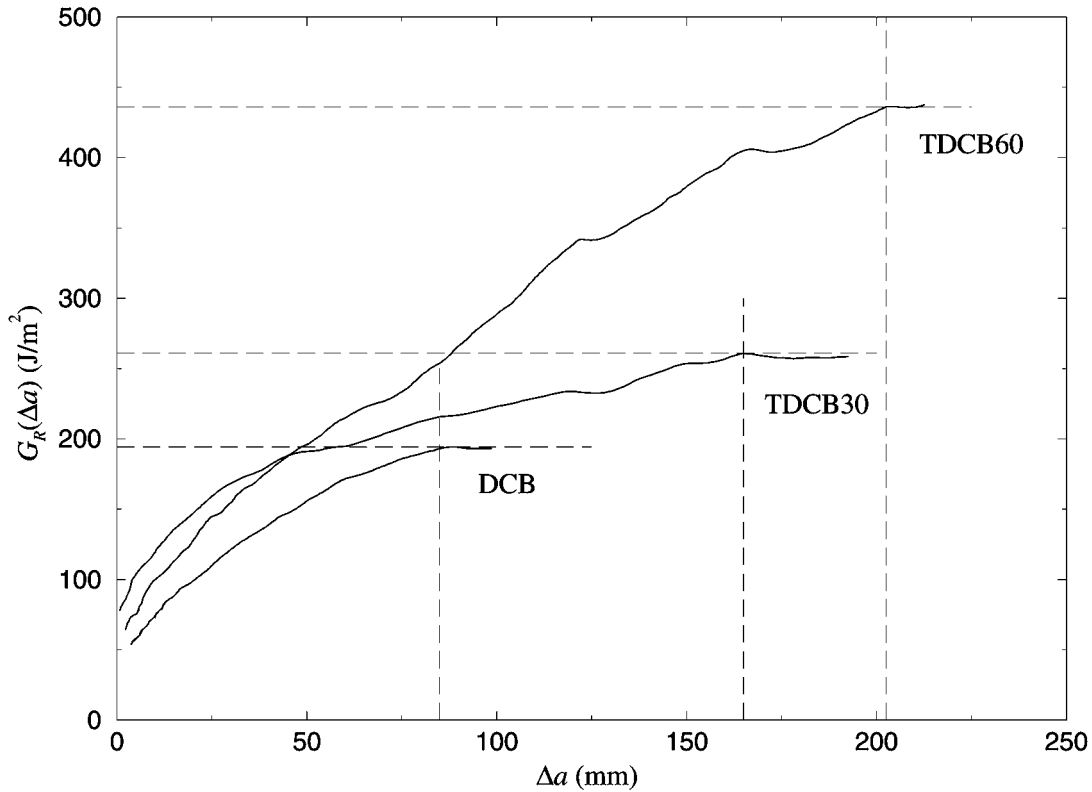


Figure 4. R -curve behaviors measured on a DCB, a TDCB30 and a TDCB60 specimen (respectively DCB-04, TDCB30-05 and TDCB60-03). The horizontal asymptotic line that starts at the crack length increment Δa_c corresponds to the critical value of the resistance to crack growth G_{RC} and is related to the postpeak crack propagation.

successive profiles (along the y direction) was chosen to increase as a geometrical series. For each map, the first profile ($y = 0$) is sampled in the immediate vicinity of the initial straight notch and corresponds approximatively to a zero roughness profile. The vertical resolution is estimated to be of the order of $5 \mu\text{m}$ from the height differences between two successive sampling along the same line. Horizontal resolutions along x and y -axis are about $2 \mu\text{m}$.

3. Morphology of crack surfaces: anomalous scaling

Many studies have been devoted to the statistical characterization of the morphology of tensile fracture surfaces in very different types of materials such as metals (Bouchaud et al., 1990; Dauskardt et al., 1990; Imre et al., 1992), ceramics (Mecholsky et al., 1989; Måløy et al., 1992), glass (Daguier et al., 1997), various rocks (Schmittbuhl et al., 1993, 1995b), sea ice (Weiss, 2001a), or various species of wood (Engøy et al., 1994; Morel et al., 1998). Despite different material natures and loading conditions, the fracture surfaces exhibit self-affine scaling properties in a large range of lengthscales (see Bouchaud, 1997 for a review) characterized by a scaling exponent $\zeta_{\text{loc}} \simeq 0.80$, which corresponds to the Hurst exponent, also called local roughness exponent. This robustness of the results seems to support the idea that the local roughness exponent is a universal value (Bouchaud et al., 1990), i.e., independent of the

Table 1. Results of the roughness analysis and of the fit of the experimental R -curve. The error bars are estimated to be 0.05 for the local roughness exponent ζ_{loc} , 0.10 for the global roughness exponent ζ and 0.20 for the dynamic exponent z . The average value of the scaling exponent $(\zeta - \zeta_{loc})/z$ obtained from the roughness analysis is estimated as to 0.20 ± 0.12 .

Specimen label	Roughness analysis					Fit of the R -curves			
	ζ_{loc}	ζ	z	y_{sat} (mm)	ξ_{max} (mm)	G_{RC} (J/m^2)	Δa_c (mm)	2γ (J/m^2)	$(\zeta - \zeta_{loc})/z$
DCB-01						171	43	10.2	0.21
DCB-02	0.80	1.05	1.40			273	56	10.5	0.32
DCB-03	0.83	1.10	2.20	98	4.8	310	110	12.1	0.29
DCB-04	0.77	1.10	2.00	87	14.4	193	85	9.8	0.43
DCB-05	0.77	1.05	2.10	96	8.3	299	114	9.8	0.32
DCB-06						193	48	10.2	0.30
DCB-07	0.82	1.20	1.80	108	5.4				
DCB	0.80	1.10	1.90	97	8.2	240	76	10.4	0.31
TDCB30-01						430	190	11.8	0.40
TDCB30-02						313	139	10.8	0.27
TDCB30-03						157	63	10.1	0.41
TDCB30-04						133	49	8.4	0.23
TDCB30-05	0.80	1.20	1.40			261	200	9.2	0.23
TDCB30	0.80	1.20	1.40			260	128	10.1	0.31
TDCB60-01						268	49	10.6	0.22
TDCB60-02	0.78	1.20	2.00	156	17.5				
TDCB60-03	0.83	1.45	1.70			436	203	12.7	0.55
TDCB60-04						192	37	9.4	0.23
TDCB60-05	0.84	1.05	1.60	98	11.7	269	148	8.1	0.23
TDCB60-06	0.80	1.10	1.60	181	6.0				
TDCB60	0.81	1.20	1.70	145	11.7	291	134	10.2	0.31
Global Average	0.80	1.15	1.78					10.2	0.31 ± 0.07

fracture mode and of the material. A physical mechanism for the origin of the local roughness exponent has been recently proposed by Hansen and Schmittbuhl (2003). It relies on a stress controlled percolation process into the damage zone. Nevertheless, if the value of the local roughness exponent ζ_{loc} seems universal, it has been shown that the crack development in quasi-brittle materials has two properties: first it is anisotropic, i.e., different in the crack propagation direction and transverse to it (Schmittbuhl et al., 1994); second it shows a growth during the propagation with two regimes: a first fast growth and a second slow evolution that lasts very long before it saturates because of the finite size of the sample (López and Schmittbuhl, 1998; Morel et al., 1998).

Indeed, if the roughness of the crack surfaces is characterized by the root mean square of the height fluctuations $\Delta h(l, y)$ estimated over a window of size l along the x axis (i.e., along a profile) and at a distance y from the initial notch, the roughness development exhibits particular scaling properties, called *anomalous scaling* in the statistical physics literature (Schroeder et al., 1993; Das Sarma et al., 1994; López and Rodríguez, 1996; López et al., 1997), such as

$$\Delta h(l, y) \simeq A \begin{cases} l^{\zeta_{loc}} \xi(y)^{\zeta - \zeta_{loc}} & \text{if } l \ll \xi(y) \\ \xi(y)^{\zeta} & \text{if } l \gg \xi(y) \end{cases}, \quad (3.1)$$

where $\xi(y)$ corresponds to the self-affine cross-over length along the x -axis below which the profile appears to be self-affine, i.e., where the scaling of the height fluctuations is driven by the local roughness exponent ζ_{loc} , $\Delta h(l \ll \xi(y), y) \sim l^{\zeta_{loc}}$, while for lengthscales $l \gg \xi(y)$, the magnitude of the roughness behaves as $\Delta h(l \gg \xi(y), y) \sim \xi(y)^{\zeta}$ which means that it is independent of the scale l but grows with the distance to the notch. The exponent ζ is called global roughness exponent and is different and independent of the local one (López et al., 1997). Moreover, the self-affine correlation length $\xi(y)$ evolves as a function of the distance to the initial notch y such as $\xi(y) \sim y^{1/z}$ where z is called dynamic exponent. Note that the term: dynamic exponent, comes from the fact that anomalous scaling was initially formulated for kinetic interface roughening where time is considered instead of the position y . Nevertheless, fractures of all specimens were observed at an approximately constant crack speed and so, we assumed a linear relationship between the position y of the profiles and the crack propagation time t .

Description of anomalous scaling of quasi-brittle fracture surfaces requires three scaling exponents: the universal local roughness exponent ζ_{loc} , the global roughness exponent ζ and the dynamic exponent z . The two last have been shown to be material dependent parameters (López and Schmittbuhl, 1998; Morel et al., 1998; Morel et al., 2002b). Note that in Equation (3.1), A is also a material dependent constant.

3.1. DETERMINATION OF THE LOCAL ROUGHNESS EXPONENT ζ_{loc}

From topographic profiles, the local roughness exponent ζ_{loc} , is computed using four statistical methods: the root mean square and max-min difference variable bandwidth methods (Schmittbuhl et al., 1995a; Bouchaud, 1997), the power spectrum method (Schmittbuhl et al., 1995a) and the averaged wavelet coefficient method (Simonsen et al., 1998). All these methods were applied for the roughness analysis, but only results obtained with the root mean square method will be reported here to illustrate the scaling of fracture surfaces.

A reliable estimate of the local roughness exponent ζ_{loc} can be obtained from profiles located far from the notch (i.e., $y \gg 0$). Indeed, according to Equation (3.1), self-affine scaling properties are expected for a large range of lengthscales. Thus, with the root mean square method, the roughness $\Delta h(l)$ computed along a topographic profile (i.e., at a given distance y from the initial notch) will to scale as:

$$\Delta h(l, y = cte) \sim \begin{cases} l^{\zeta_{loc}} & \text{if } l \ll \xi(y) \\ const. & \text{if } l \gg \xi(y) \end{cases}, \quad (3.2)$$

From Fig. 6 (circle symbols), for lengthscales $l \ll \xi(y)$, the fit of the roughness (rms) with a power such as proposed in (3.2) allows to estimate a local roughness exponent $\zeta_{loc} \simeq 0.8$

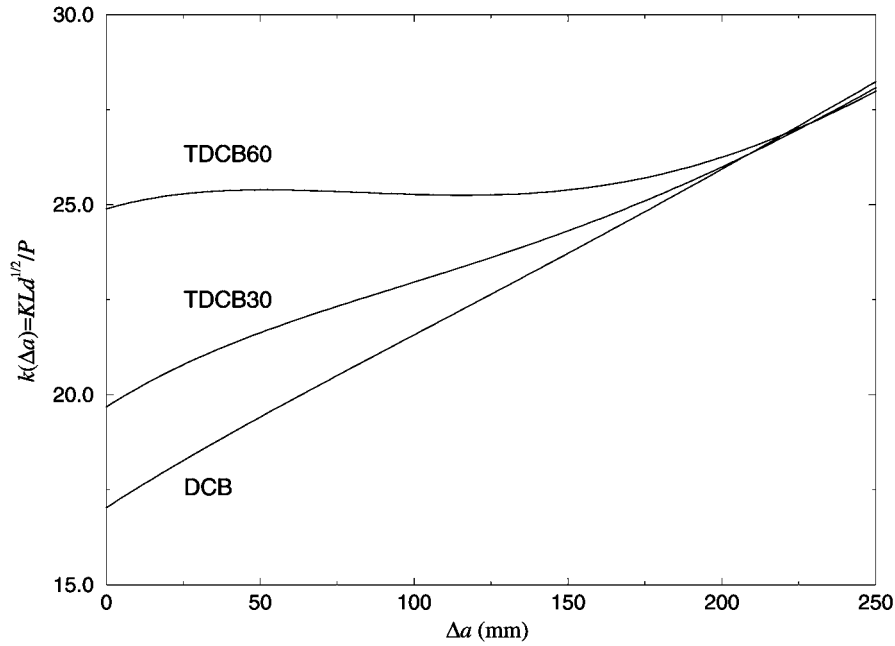


Figure 5. Dimensionless stress intensity factor function $k(\Delta a)$ vs crack length increment Δa for a unity load P obtained from a finite element method in case of TDCB60, TDCB30 and DCB specimens.

which is in good agreement with the conjecture of a universal exponent (Bouchaud et al., 1990). Similar results have been obtained for all tested specimens (Table 1). However, it can be observed in Fig. 6 that a filtering of the raw profiles is necessary. Indeed a different behavior is observed on raw data (diamond symbols) for the smallest lengthscales and corresponds a roughness exponent equal to 0.5. This regime at small lengthscales has to be related to the fact that, during the fracture process in wood, cells or small groups of cells might be not fully pulled apart from the crack surface and appear from a microscope observation as a set of wires stuck to the crack surface. These local perturbations of the crack surface are randomly distributed on the fracture surface. They are seen by the optical profiler since they cut the laser beam but are not representative of the real fracture surface. Indeed, previous roughness analysis that were performed on wood fractured surfaces recorded with a mechanical profiler (Morel et al., 1998), have shown a single self-affine domain which the lower cut-off l_o was closer to the cell width, i.e., approximately $25 \mu\text{m}$. The main difference between the optical and the mechanical profiler is that the latter searches for contact with the fracture surface. It uses a force that is sufficient to squeeze the wires of cells on the surface. On the contrary the optical profiler does not modify the position of the cell wires and measures non realistic heights of the surface. In order to correct for this artifact we filtered each profile using wavelet transform. Wavelet coefficients corresponding to small lengthscales of the profiles were set to zero like in high pass wavelet filters (Press et al., 1992). As shown in Fig. 6, the roughness obtain after filtering exhibit self-affine scaling properties over a large range of lengthscales and the lower cut-off is approximately equal to the step of sampling, i.e., $25 \mu\text{m}$.

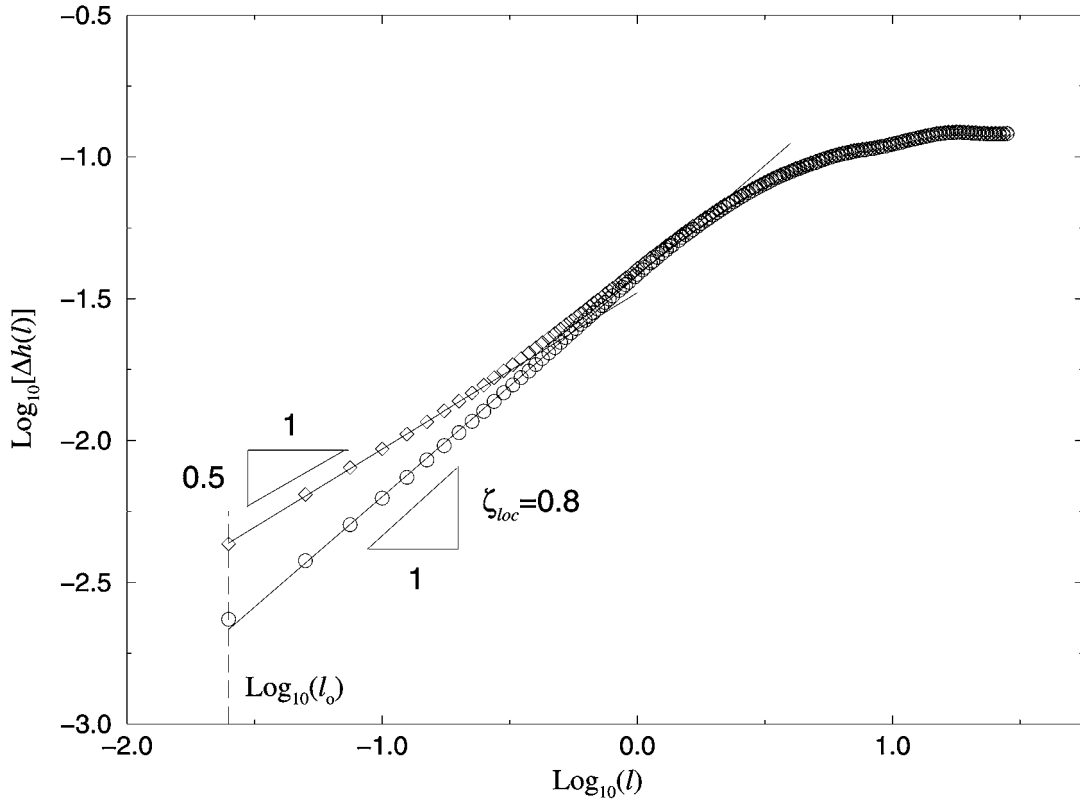


Figure 6. Roughness (rms) $\Delta h(l)$ for a profile far from the notch, i.e., $y \gg 0$. Diamonds and circles correspond respectively to the roughness obtained before and after high pass wavelet filtering of the profile. The straight line corresponds to the power law $\Delta h(l) \sim l^{\zeta_{loc}}$, and gives a determination of the local roughness exponent $\zeta_{loc} = 0.80$ (DCB-04 specimen).

3.2. DEVELOPMENT OF THE ROUGHNESS: GLOBAL ROUGHNESS AND DYNAMIC EXPONENT

As previously observed on fracture surfaces of two quasi-brittle materials, granite (López and Schmittbuhl, 1998) and wood (Morel et al., 1998), the roughness development exhibits particular scaling properties, called *anomalous* scaling (3.1).

An illustration of this scaling can be seen in Fig. 7, where the roughness $\Delta h(l, y)$ is plotted as a function of the distance to initial notch y for different lengthscales l in the case of a TDCB60 specimen (TDCB60-05). The upper line correspond to a fit of the roughness growth for a large lengthscale $l = L/2 = 30$ mm. This lengthscale has been chosen to be larger than the self-affine correlation length $\xi(y)$ and this whatever the distance to initial notch y is. Thus, according to (3.1) and due to the fact that $\xi(y) \sim y^{1/z}$, the slope of this fit provides an estimate of the ratio $\zeta/z \simeq 0.68$. The fit is performed for distances to initial notch y between y_{min} and y_{sat} . The distances smaller than y_{min} correspond to the first millimeters of the fracture surface close to the initial notch and for which the kinetic of crack propagation is not completely established while, for the distances greater than y_{sat} , the magnitude of the roughness saturates. This stationary regime of the roughness can be explained by the fact that, for distances $y \gg y_{sat}$, the self-affine correlation length $\xi(y)$ has reached a maximum value

ξ_{\max} , $\xi(y \gg y_{\text{sat}}) = \xi_{\max}$, and hence the roughness $\Delta h(l, y \gg y_{\text{sat}})$ becomes independent of the distance to initial notch y and saturates, according to (3.1) as :

$$\Delta h(l, y \gg y_{\text{sat}}) \simeq A \begin{cases} l^{\zeta_{\text{loc}}} \xi_{\max}^{\zeta - \zeta_{\text{loc}}} & \text{if } l \ll \xi_{\max} \\ \xi_{\max}^{\zeta} & \text{if } l \gg \xi_{\max} \end{cases} \quad (3.3)$$

In Fig. 7, the lower line corresponds to a fit of the roughness measured for the smallest length-scale, $l = l_o = 25 \mu\text{m}$. It appears that, even for small lengthscales, the roughness $\Delta h(l, y)$ increases like a power law as a function of the distance y to initial notch. The slope of the fit is 0.29 and gives, according to anomalous scaling (3.1), an estimate of the ratio $(\zeta - \zeta_{\text{loc}})/z$. For an intermediate lengthscale l^* , two roughness growth regimes can be observed (Fig. 7). For distances $y \ll y^*$ (where y^* is defined as the distance to initial notch for which the self-affine correlation length $\xi(y^*)$ corresponds to the observed lengthscale l^* : $\xi(y^*) = l^*$), the roughness growth regime is similar to the one defined by the upper line (a). Indeed, for distances $y \ll y^*$ the lengthscale l^* is greater than the self-affine correlation length $\xi(y \ll y^*)$ and so, according to (3.1), the roughness is expected to scale as $\Delta h(l^* \gg \xi(y), y \ll y^*) \sim y^{\zeta/z}$. Moreover, for distances $y \gg y^*$, the lengthscale l^* becomes smaller than the self-affine correlation length, $l^* \ll \xi(y \gg y^*)$ and so, according to (3.1), the roughness growth regime is similar to the one of the lower line (b), i.e., $\Delta h(l^* \ll \xi(y), y \gg y^*) \sim y^{(\zeta - \zeta_{\text{loc}})/z}$. This dependence of the magnitude of the roughness on distance y to initial notch is an illustration of the anomalous scaling. Note that such a behavior has been observed on all tested specimens.

Thus, the roughness of fracture surfaces that start from a straight notch, shows a first zone where the magnitude of the roughness increases as a function of the distance y to initial notch and, far from the notch, for distances $y \gg y_{\text{sat}}$, it can be observed a steady state of the roughness development where the magnitude of the roughness saturates.

Within the framework of López et al. (1997), an accurate estimation of the global roughness exponent ζ and of the dynamic exponent z can be obtained from the determination of the scaling function $g(u)$ as $g(l/y^{1/z}) = \Delta h(l, y)/l^{\zeta}$. From anomalous scaling (3.1), $g(u)$ is expected to scale as:

$$g(u) \sim \begin{cases} u^{-(\zeta - \zeta_{\text{loc}})} & \text{if } u \ll 1 \\ u^{-\zeta} & \text{if } u \gg 1. \end{cases} \quad (3.4)$$

For each fracture surfaces, the exponent ζ and z are estimated on the basis of the scaling function $g(u)$ (3.4) from the collapse of all the profiles ranging between y_{min} and y_{sat} . Figure 8 shows the data collapses obtained respectively in the case of a DCB, TDCB30 and TDCB60 specimen. It can be seen that the collapses are in good agreement with the scaling function (3.4). An important aspect is the non flat and horizontal behavior for small u ($u \ll 1$) which clearly shows anomalous scaling, i.e., $\zeta \neq \zeta_{\text{loc}}$. The values of ζ and z obtained from the least scattering of the collapses are reported in Table 1 for DCB, TDCB30 and TDCB60 specimens. The main result of these collapses is that the global roughness exponent seems independent of the specimen shape. As shown in Table 1 an average value $\zeta = 1.15 \pm 0.10$ is obtained. Hence, the global roughness exponent ζ seems to be material dependent, i.e., independent of the specimen geometry and independent of the specimen size (as previously shown in Morel et al., 1998). Moreover, in spite of the scattering of the dynamic exponent, z seems also independent of the specimen shape. Note that z is expected to be large for material like wood where growth rate of the roughness is controlled by the shape of the cells and more specifically their length. Indeed, the roughness is not expected to evolve on lengthscale along

crack propagation direction smaller than the cell length which is much larger than the cell width.

As reported in Table 1, the distances y_{sat} are greater in TDCB60 than in TDCB30 specimens and the same observation can be made between TDCB30 and DCB specimens. The *average* compliance of the specimens is having an influence on the distance y_{sat} for which the saturation of the roughness occurs: the higher the *average* compliance of the specimen, the larger the zone of roughness growth. Moreover, the evolution of the self-affine correlation length with the distance y : $\xi(y) \sim y^{1/z}$, appears as independent of the specimen shape (the dynamic exponent z being independent of the specimen shape). Accordingly longer maximum self-affine correlation lengths ξ_{max} are observed for specimens with a larger compliance, as shown in Table 1. As a consequence of Equation (3.3), the maximum roughness magnitude of fracture surfaces $\Delta h(l, y \gg y_{\text{sat}})$ increases with the *average* compliance of the specimens. If the global roughness exponent ζ and the dynamic exponent z are material dependent constant, the zone of roughness growth and the maximum magnitude of the roughness are larger in specimens of higher compliance.

4. Roughening of crack surfaces and R-curve behavior

Many attempts were made in the past to establish connections between the fracture toughness of materials and either the fractal dimension (Mosolov, 1993; Carpinteri, 1994; Balankin, 1996; Borodich, 1997; Bažant, 1997; Weiss, 2001b) or relevant lengthscales (Bouchaud and Bouchaud, 1994). Nevertheless, all these connections were established on the basis of a description of the roughness that does not take into account the development of fracture surfaces (such as anomalous scaling, see Section 3).

4.1. FRACTURE CRITERION IN THE CASE OF AN ANOMALOUS SCALING

Within the framework of an equivalent linear elastic problem, a fracture criterion, linking the elastic energy release rate G at the macroscale and the roughening of the crack at the microscale, was recently proposed (Morel et al., 2000, 2002b):

$$G = 2\gamma \frac{\psi(y)}{L}, \quad (4.1)$$

where γ is the so-called specific surface energy and the ratio $\psi(y)/L$ can be considered as a ‘roughness factor’ translating the roughening of the crack surface. It is precisely the ratio of the length of a *virtual* crack front over its projected length L (i.e., the specimen width). This virtual front is defined as parallel to the initial notch (along x axis) and with a roughness only out of the average fracture plane (x, y). Its roughness can be defined from the function $\Delta h(l, y)$ (3.1) at a fixed position y from the initial notch. According to anomalous scaling (Equation (3.1)), the estimate of the real length ψ of the virtual front, which corresponds to the length of a self-affine curve (Morel et al., 2000; 2002b), leads to the following expression of the energy release rate:

$$G_R(\Delta a) \simeq 2\gamma \begin{cases} \sqrt{1 + \left(\frac{AB^{\zeta-\zeta_{\text{loc}}}}{l_o^{1-\zeta_{\text{loc}}}}\right)^2 \Delta a^{2(\zeta-\zeta_{\text{loc}})/z}} & \text{if } \Delta a \ll \Delta a_{\text{sat}} \\ \sqrt{1 + \left(\frac{A}{l_o^{1-\zeta_{\text{loc}}}}\right)^2 \xi_{\text{max}}^{2(\zeta-\zeta_{\text{loc}})}} & \text{if } \Delta a \gg \Delta a_{\text{sat}}, \end{cases} \quad (4.2)$$

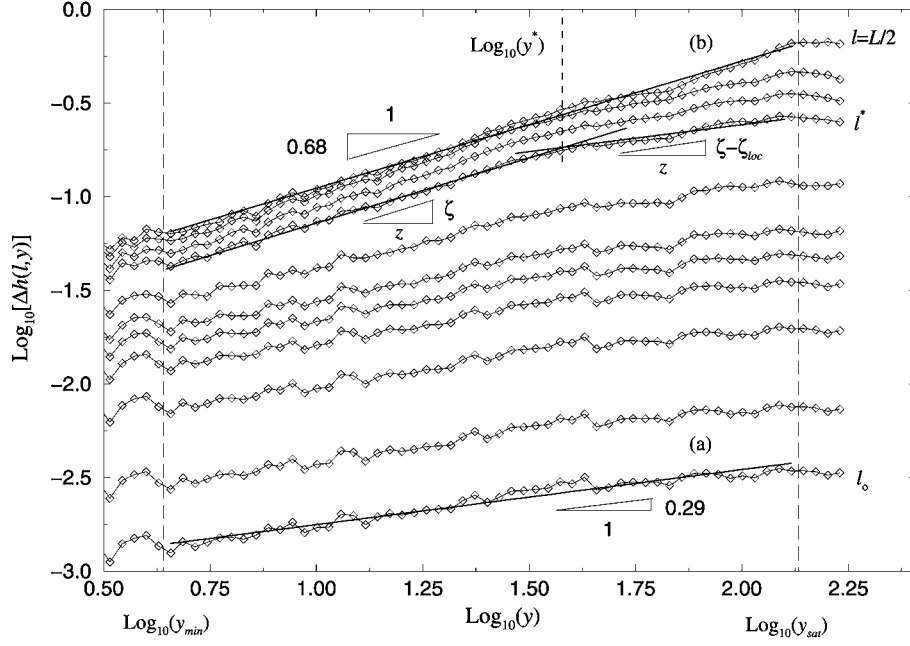


Figure 7. Roughness (rms) $\Delta h(l, y)$ vs distance to initial notch y for a TDCB60 specimen (TDCB60-05) computed over lengthscales l ranging from $l = 0.025$ mm to 30 mm. The continuous line (a) corresponds to the fit of the roughness growth $\Delta h(l, y) \sim y^{\zeta - \zeta_{loc}/z}$ for the smallest lengthscale $l = 0.025$ mm while the line (b) is the fit of the roughness growth at large lengthscales (i.e., $l \gg \xi(y)$): $\Delta h(l, y) \sim y^{\zeta/z}$.

where the crack length increments Δa and Δa_{sat} defined from the initial notch, correspond respectively to the crack positions y and y_{sat} defined in Section 3. The term B in (4.2) is a material dependent constant which arises from the power law relationship between the self-affine correlation length ξ and the crack length increment Δa (or distance to initial notch): $\xi(\Delta a) = B \Delta a^{1/z}$. Thus, in the zone where the roughness grows, i.e., for $\Delta a \ll \Delta a_{\text{sat}}$, the fracture equilibrium leads to an energy release rate function of the crack length increment Δa (4.2) which is a resistance curve (R -curve). The square root terms in (4.2) are dimensionless and correspond to the roughness factor $\psi(y)/L$. When the crack length increment is large, i.e., for $\Delta a \gg \Delta a_{\text{sat}}$ which corresponds to the steady state of the roughness, the resistance to fracture growth becomes independent of the crack advance because the self-affine correlation length has reached its maximum value ξ_{max} (Equation 3.3). This induces a saturation of the real length ψ of the virtual front: $\psi(\Delta a \gg \Delta a_{\text{sat}}) = \psi_{\text{max}}$. Thus, for large crack length increments $\Delta a \gg \Delta a_{\text{sat}}$, the fracture equilibrium leads to a post R -curve propagation at constant resistance and can be defined as a *critical* resistance to crack growth: $G_R(\Delta a \gg \Delta a_{\text{sat}}) = G_{RC}$.

Note that, the term l_0 in (4.2) is the lower cutoff of the fractal range of the virtual front. This lower bound, which necessarily exists, at least at the atomic scale (Weiss, 2001b), should be theoretically the characteristic size of the smallest microstructural element relevant for the fracture process. Such a lower bound, in the estimate of the length of a self-affine curve, provides a fracture energy (4.2) in agreement with the classical dimensions of LFM (see also Weiss, 2001b) contrary to those obtained in Carpinteri (1994), Borodich (1997) and Bažant (1997) where an unconventional definition of fracture energy, called *fractal fracture energy*, is required.

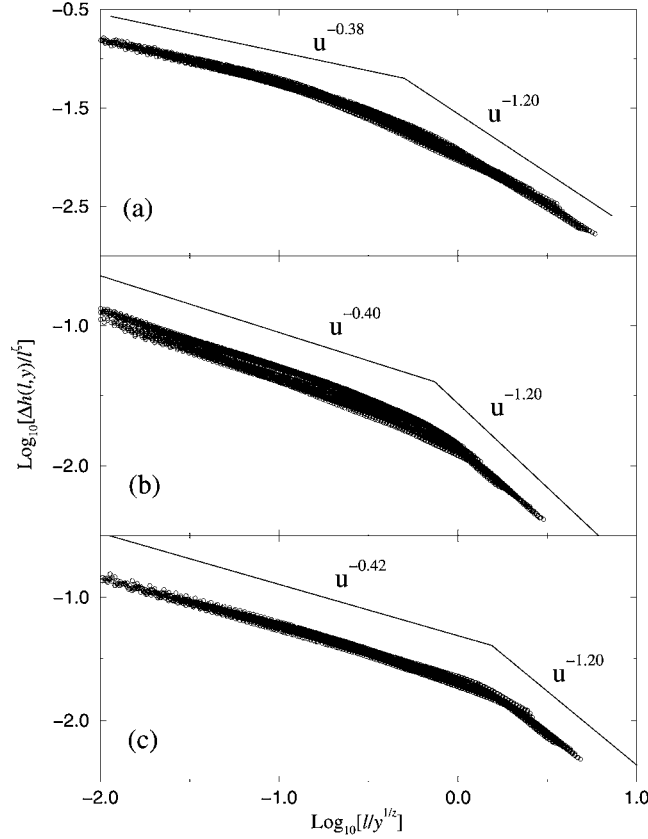


Figure 8. Data collapses in the case of a DCB (a), TDCB30 (b) and TDCB60 (c) specimen. The nonzero slope at small values of $l/y^{1/2}$ emphasizes the dependence on distance from initial notch y of the roughness magnitude.

4.2. FIT OF THE EXPERIMENTAL R -CURVES

In Fig.9 are plotted some examples of the experimental resistances to crack growth obtained respectively in the case of a DCB, a TDCB30 and TDCB60 specimen. The resistance curves are fitted with the R -curve (4.2) keeping three free parameters: the specific surface energy 2γ , the ratio $A/l_o^{1-\zeta_{loc}}$ and the scaling exponent $(\zeta - \zeta_{loc})/z$. As shown in Fig. 9, the expected R -curve behavior (4.2) provides a good description of the increase of the experimental resistances to crack growth. The values obtained from the fits of the R -curves are reported in Table 1. The scaling exponent $(\zeta - \zeta_{loc})/z$, which drives the evolution of the experimental resistance to crack growth G_R as a function of the crack advance Δa , seems independent of the specimen geometry. Moreover, in spite of the strong scattering of experimental results for wood (which is due to the natural variability of this material), the average value $(\zeta - \zeta_{loc})/z = 0.31 \pm 0.07$ obtained from the fits at macroscopic scale is quite close to the one obtained from the roughness analysis at microscopic scale, $(\zeta - \zeta_{loc})/z = 0.20 \pm 0.12$ (Table 1). Nevertheless, the fact the $(\zeta - \zeta_{loc})/z$ scaling exponents obtained from the roughness analysis are slightly smaller than those obtained from the R -curve fits can be partly explained by the filtering operation on the topographic profiles (Section 3.1). Indeed, it appears that the high pass wavelet filter induces a light overestimation of the local roughness exponent ζ_{loc} while the global roughness exponent ζ and the dynamic exponent z are not affected by this filtering.

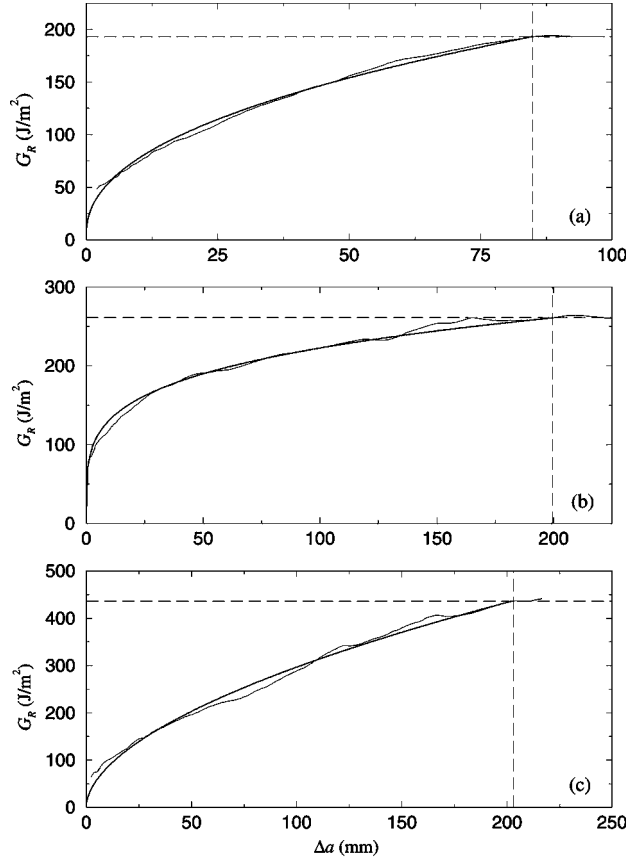


Figure 9. Fits of experimental R -curves obtained from (4.2) in the case of the DCB-04 (a), TDCB30-05 (b) and a TDCB60-03 (c) specimens.

Hence, such an overestimation of the ζ_{loc} exponent can induce a light underestimation of the scaling exponent $(\zeta - \zeta_{loc})/z$ during the analysis of the roughness development. On the other hand, it can be seen in Table 1 that the critical crack length increment Δa_c that corresponds to the *end* of the experimental R -curves (for which the resistance does not follow the R -curve but remains constant and equal to the critical value $G_{RC} = G_R(\Delta a \geq \Delta a_c)$) are quite close to the crack advance $\Delta a_{sat} = y_{sat}$ for which the steady state (3.3) of the roughness occurs. Indeed, according to Equation (4.2), for crack length increments $\Delta a \gg \Delta a_{sat}$, the resistance is expected to saturate as $G_R(\Delta a \gg \Delta a_{sat}) = const.$ Thus, notwithstanding the scatter of the experimental results, the similarities between the fitted and measured scaling exponent $(\zeta - \zeta_{loc})/z$ and between the crack length increments Δa_c and Δa_{sat} , seem to confirm the initial idea according to which the microscopic roughening of crack surfaces is expected to reflect the macroscopic fracture behavior of materials.

The values of the specific surface energy 2γ (Table 1) obtained from the fit of the experimental R -curves are close to those obtained in Morel et al. (2002b) for another wood species. These values of 2γ if compared to the critical energy release rates G_{RC} indicate a strong toughening mechanism in wood (i.e., $G_{RC} \gg 2\gamma$). Moreover, as previously mentioned in Section 3.2, the fact that the maximum magnitude of the roughness (i.e., for $y \gg y_{sat}$) appears

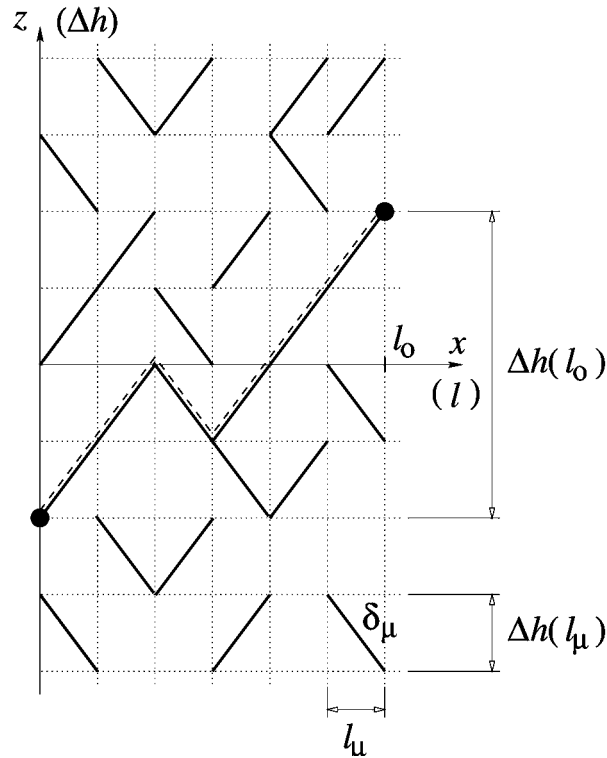


Figure 10. Schematic representation of an anomalous microcracking along the x axis. The average magnitude of microcracks $\Delta h(l_\mu)$ is assumed to follow an anomalous scaling (4.3). The front line (dashed line) takes place by microcrack coalescence. The two black points correspond to those measured during the topographic record, i.e., with a step of sampling corresponding to the lengthscale l_o . The average height difference between two successive recorded points $\Delta h(l_o)$ scales according to the anomalous scaling (3.1).

as a function of the average compliance of the specimen is in agreement with the fact that the critical energy release rates G_{RC} are higher in TDCB60 specimens than in DCB specimens.

However, the fit of the experimental resistance curves needs the use overestimated ratios $A/l_o^{1-\zeta_{loc}}$ if compared to those obtained from the roughness analysis. If one notes Φ_R the ratio of the values $A/l_o^{1-\zeta_{loc}}$ obtained from the fit of the experimental R -curves over those obtained from the roughness analysis, it appears that $10 \leq \Phi_R \leq 20$. Moreover, the ratio $A/l_o^{1-\zeta_{loc}}$ can be seen as the tangent of the average local angle along the virtual crack front. Hence, such large Φ_R values emphasize the strong magnification of the roughness needed to obtain good fits of the experimental R -curves. Note that, the experimental value of the material constant A (3.1) can be estimated from experimental lengths of topographic profiles while the value of l_o , fixed by the step of sampling of the topographic profiles ($l_o = \Delta x = 25 \mu\text{m}$), corresponds to the cell width of wood (Section 2). In order to explain such overestimated ratios $A/l_o^{1-\zeta_{loc}}$, the first idea consists to consider a lower cutoff l_o smaller than the step of sampling of the topographic profiles. Indeed, during the fracture process of wood, some cell walls break revealing a microstructure at smaller lengthscales. However, the average lengthscale l_o , deduced from the ratios $A/l_o^{1-\zeta_{loc}}$ is very small and unreasonable with regards to the wood microstructure.

As a consequence, if the connection between roughening of crack surfaces and material fracture properties (4.2) allows to obtain an estimate of the scaling of the experimental resistance to crack growth G_R , it seems to not reflect the magnitude of this resistance. Note

that, this insufficiency of the connection between self-affine nature of crack surfaces and the material fracture properties (4.2) was expected owing to the fact that this connection is based on the energy released by a single rough crack. Indeed, such an assumption is oversimplified for quasi-brittle materials because of the existence of a fracture process zone where energy dissipation which is very different from that of a tip of a single elastic crack. Though the energy dissipated in the fracture process zone is impossible to measure experimentally, a possible method to describe the entire R -curve behavior consist to rewrite the connection (4.2) taking into account the energy dissipated by a set of virtual microcracks instead of that dissipated by the single main crack.

4.3. ENERGY RELEASED BY AN ANOMALOUS MICROCRACKING

As previously mentioned, the real value of the lower cutoff l_o of the self-affine range might be smaller than the cell width. Indeed, because the fracture process, the fracture of cell walls shows a microstructure at smaller lengthscales. Accordingly, it exists cracked surfaces which are not measured and subsequently not taken into account in the estimate of the energy release rate (4.2). An alternative description is to consider a set of microcracks that develop at a lengthscale smaller than the cell width l_o . It is rather intuitive to imagine the final crack surface as the path of a fracture front that advances through a distributed set of microcracks by a coalescence process (Fig. 10). Let us note $l_\mu = l_o/\alpha$ (where $\alpha \geq 1$ is a constant) the lengthscale corresponding to the average width of the microcracks along the x axis and, in order to be in agreement with the observed scale invariance of the main crack, consider that the microcracking scales according to the anomalous scaling (3.1) as

$$\Delta h(l_\mu, y) \simeq A \begin{cases} l_\mu^{\zeta_{loc}} \xi(y)^{\zeta - \zeta_{loc}} & \text{if } y \ll y_{sat} \\ l_\mu^{\zeta_{loc}} \xi_{max}^{\zeta - \zeta_{loc}} & \text{if } y \gg y_{sat}. \end{cases} \quad (4.3)$$

Moreover, let us consider that the number n of the microcracks which nucleate at the lengthscale l_μ (Fig. 10) remains approximately constant for the large distances to initial notch $y \gg 0$. Indeed, it is not reasonable to consider such an assumption at the onset of fracture, i.e., for the distances y close to 0.

From this theoretical configuration of an anomalous microcracking, it is possible to use the fracture criterion (4.1) and substitutes the length of the virtual crack front $\psi(y)$ by the length $\psi_\mu(y)$ which is the developed length of the microcracks cloud along the x axis. Therefore, the length δ_μ of a microcrack can be estimated from (4.3) as

$$\delta_\mu(y \ll y_{sat}) \simeq l_\mu \sqrt{1 + \left(\frac{A \xi(y)^{\zeta - \zeta_{loc}}}{l_\mu^{1 - \zeta_{loc}}} \right)^2} \quad (4.4)$$

and, hence, the developed length $\psi_\mu(y)$ of the microcracks cloud along the x axis can be expressed as: $\psi_\mu(y) = (L/l_\mu)n\delta_\mu$. Thus, substituting $\psi_\mu(y)$ into the fracture criterion (4.1) yields the energy release rate expression:

$$G_\mu(\Delta a \ll \Delta a_{sat}) \simeq 2n\gamma \sqrt{1 + \left(\frac{A}{l_\mu^{1 - \zeta_{loc}}} \right)^2} \xi(y)^{2(\zeta - \zeta_{loc})} \quad (4.5)$$

which is approximatively of the same form that the R -curve behavior (4.2) obtained from a single rough crack. If an anomalous microcracking exists, the R -curve behavior described by

(4.2) should be equal to the energy released by the microcracks (4.5): $G_R(\Delta a) = G_\mu(\Delta a)$. Thus, from latter equality, it appears possible to estimate the ratio Φ_R (defined in Section 4.2 as the ratio of the overestimated value $A/l_o^{1-\zeta_{loc}}$ induced by the fit of the experimental R -curve over the one obtained from the roughness analysis) as

$$\Phi_R(\Delta a) = n \alpha^{1-\zeta_{loc}} \sqrt{1 + \frac{n^2 - 1}{n^2} \left(\frac{l_\mu^{1-\zeta_{loc}}}{A \xi (\Delta a)^{\zeta - \zeta_{loc}}} \right)^2} \quad (4.6)$$

From (4.6), the ratio Φ_R (which has been defined as a magnification factor of the main crack roughness in Section 4.2) is function of the crack length increment Δa . In fact, Φ_R decreases with the crack advance. This dependence of Φ_R on Δa appears inconsistent with the initial definition in which Φ_R is a constant. Nevertheless, for large crack length increment, i.e., $\Delta a \gg 0$, the ratio Φ_R tends toward the asymptotic value

$$\Phi_R(\Delta a \gg 0) \simeq n \alpha^{1-\zeta_{loc}} \quad (4.7)$$

Thus, from (4.7), the values of Φ_R obtained from the fit of experimental R -curve (i.e., $10 \leq \Phi_R \leq 20$) induce a reasonable microcracking configuration in which about 10 microcracks nucleate at a lengthscale $l_\mu \simeq 2.5 \mu\text{m}$. Though this approach must be considered as a theoretical one, the results obtained for n and α seem a sane assumption for the fracture process of a quasi-brittle material such as wood.

5. Conclusion

Mode I fracture tests performed on three different shapes of wood specimens (DCB, TDCB30 and TDCB60) have shown pronounced resistance curve (R -curve) behaviors for all specimen geometries. Nevertheless, the critical resistances G_{RC} and their corresponding crack length increment Δa_c (defined respectively as the values of the resistance and of the crack length increment at the end of the R -curve behavior (i.e., before the plateau of the resistance at the peak load) appear dependent on the *average* compliance of the specimens. We argue that this dependence of the critical resistance G_{RC} and crack length increment Δa_c on the specimen compliance, can be explained by the behavior of the stress intensity factor (for the same load and crack length). Indeed the stress intensity factor increases as a function of the *average* compliance of the specimens. Accordingly fracture process zones extend on larger distances when the specimen compliance is higher. Hence, the equivalent linear elastic crack length increment Δa_c and the release of stored energy G_{RC} by such a fracture process zone, are expected to increase with the average compliance of the specimens.

The complete 3D roughness analysis of numerous crack surfaces obtained from these fracture tests has been performed. We show that the anomalous scaling ansatz provides an accurate description of the roughness development of crack surfaces. The scaling exponents (especially the global roughness exponent ζ and the dynamic one z) are not influenced by the specimen geometry and so, appear as material dependent parameters. However, we show that if the global roughness exponent ζ and the dynamic exponent z are material dependent constant, the zone of roughness growth (i.e., for crack length increment $\Delta a \ll \Delta a_{\text{sat}}$) and the maximum magnitude of the roughness are larger for specimens of higher compliance.

On the basis of the link between the scaling of microscopic fracture roughness and macroscopic material fracture properties (Morel et al., 2000), we show that the experimental resistance curves can be fitted from the analytical expansion of the R -curve obtained from

the anomalous scaling observed for crack roughness. In spite of the usual strong scattering of the experimental results for wood, the results obtained from the fits show quite good correlations between the average fitted and measured scaling exponent $(\zeta - \zeta_{loc})/z$ and between the crack length increment Δa_c and Δa_{sat} . Moreover, the fact that the maximum magnitude of the roughness evolves as a function of the specimen compliance (which emphasizes that the real cracked surfaces are larger in TDCB60 than in DCB specimens), is in agreement with critical resistances G_{RC} that are higher in TDCB60 specimens than in DCB specimens.

However, the fit of experimental resistance curves needs the use overestimated ratios $A/l_o^{1-\zeta_{loc}}$. In other terms it requires to consider larger cracked areas compared to those estimated from the roughness analysis. As a consequence, although the connection (4.2) between roughening of crack surfaces and material fracture properties allows to obtain a correct behavior of the experimental resistance to crack growth G_R , the magnitude of this resistance is not correctly estimated. We argue that this insufficiency was expected. Indeed, this link is only based on the energy released by the tip of a single rough crack while, in quasi-brittle materials, the energy is dissipated by a process zone. A theoretical approach is proposed which consists in considering the energy released by the development of a set of microcracks with a roughness that shows anomalous scaling. The results obtained by such a theoretical approach seem reasonable if compared to the strong toughening mechanisms which take place in the fracture process of a quasi-brittle material such as wood.

Acknowledgements

We wish to thank E. Bouchaud, A. Hansen, K.J. Måløy, A. Ziv, Y. Berthaud and M. François for very fruitful discussions.

References

- Balankin, A.S. (1996). The effect of fracture surface morphology on the crack mechanics in a brittle material. *International Journal of Fracture* **76**, R63–R70.
- Bažant, Z.P., Kazemi, M.T. (1990). Size effect in fracture of ceramics and its use to determine fracture energy and effective process zone length. *Journal of the American Ceramic Society* **73** (7), 1841–1853, and references therein.
- Bažant, Z.P. (1997). Scaling of quasibrittle fracture: hypotheses of invasive and lacunar fractality, their critique and Weibull connection. *International Journal of Fracture* **83**, 41–65, and references therein.
- Borodich, F.M. (1997). Some fractal models of fracture. *Journal of the Mechanics and Physics of Solids* **45** (2), 239–259, and references therein.
- Bouchaud, E., Lapasset, G., Planés, J. (1990). Fractal dimension of fractured surfaces : a universal value ?. *Europhys. Letters* **13**, 73–79.
- Bouchaud, E., Bouchaud, J.-P. (1994). Fracture surfaces : apparent roughness, relevant lengthscales, and fracture toughness. *Physic Review B* **50** (23), 17752–17755.
- Bouchaud, E. (1997). Scaling properties of cracks. *Journal of the Physics Cond. Materials* **9**, 4319. 797–814.
- Carpinteri, A. (1994). Scaling laws and renormalization groups for strength and toughness scaling of disordered materials. *International Journal of Solids and Structure* **31** (3), 291–302.
- Daguier, P., Nghiem, B., Bouchaud, E., Creuzet, F. (1997). Pinning/Depinning of crack fronts in heterogeneous materials. *Physics of Review Letters* **78**, 1062–1065.
- Das Sarma, S., Ghaisas, S.V., Kim, J.M. (1994). Kinetic super-roughening and anomalous dynamic scaling in nonequilibrium growth models. *Physics Review E* **49** (1), 122–125.
- Dauskardt, R.H., Haubensak, F., Ritchie, R.O. (1990). On the interpretation of the fractal character of fracture surfaces. *Acta Metallica Material* **38** (2), 143–159.

- Ducourthial, E., Bouchaud, E., Chaboche, J.-L. (2000). Influence of microcracks on the propagation of macrocracks. *Computational Material Science* **19**, 229–234.
- Engøy, T., Måløy, K.J., Hansen, A., Roux, S. (1994). Roughness of two- dimensionnal cracks in wood. *Physics Review Letter* **73** (6), 834–837.
- Feder, J. (1988). *Fractals*. Plenum Press (New-York).
- Hansen, A., Schmittbuhl, J. (2003). Origin of the Universal Roughness Exponent of Brittle Fracture Surfaces: Stress-weighted Percolation in the Damage Zone. *Physics Review Letters* **90**, 045505.
- Imre, A., Pajkossy, T., Nyikos, L. (1992). Electrochemical determination of the fractal dimension of fractured surfaces. *Acta Metallica Material* **40** (8), 1819–1826.
- Lawn, B.R. (1993). *Fracture of Brittle Solids*. 2nd ed, Cambridge University Press, Cambridge, England.
- López, J.M., Rodríguez, M.A. (1996). Lack of self-affinity and anomalous roughening in growth processes. *Physics Review E* **54** (3), R2189–R2192.
- López, J.M., Rodríguez, M.A., Cuerno, R. (1997). Superroughening versus intrinsic anomalous scaling of surfaces. *Physics Review E* **56** (4), 3993–3998.
- López, J.M., Schmittbuhl, J. (1998). Anomalous scaling of fracture surfaces. *Physics Review E* **57**, 6405–6409.
- Måløy, K.J., Hansen, A., Hinrichsen, E.L., Roux, S. (1992). Experimental measurements of the roughness of brittle cracks. *Physics Review Letter* **68**, 213–215.
- Mandelbrot, B.B., Passoja, D.E., Paullay, A.J. (1984). Fractal character of fracture surfaces of metals. *Nature* **308**, 721–722.
- Mecholsky, J.J., Passoja, D.E., Feinberg-Ringel, K.S. (1989). Quantitative analysis of brittle fracture surfaces using fractal geometry. *Journal of the American Ceramic Society* **72** (1), 60–65.
- Morel, S., Schmittbuhl, J., López, J.M., Valentin, G. (1998). Anomalous roughening of wood fractured surfaces. *Physics Review E* **58** (6), 6999–7005.
- Morel, S., Schmittbuhl, J., Bouchaud, E., Valentin, G. (2000). Scaling of crack surfaces and implications for fracture mechanics. *Physics Review Letter* **85**, 1678–1681.
- Morel, S., Bouchaud, E., Valentin, G. (2002a). Size effect in fracture: Roughening of crack surfaces and asymptotic analysis. *Physics Review B* **65** (10), 104101.
- Morel, S., Bouchaud, E., Schmittbuhl, J., Valentin, G. (2002b). *R*-curve behavior and roughness development of fracture surfaces. *International Journal of Fracture* **114** (4), 307–325.
- Mosolov, A.B. (1993). Mechanics of fractal cracks in brittle solids. *Europhysics Letters* **24** (8), 673–678.
- Press, W.H., Teukolsky, S.A., Vetterling, W.T., Flannery, B.P. (1992). *Numerical Recipes*. 2nd ed., Cambridge University Press (Cambridge).
- Schmittbuhl, J., Hansen, A., Batrouni, B. (2003). Roughness of Interfacial crack front: Stress-weighted Percolation in the Damage Zone. *Physics Review Letters* **90**, 045504.
- Schmittbuhl, J., Gentier, S., Roux, S. (1993). Field measurements of the roughness of fault surfaces. *Geo. Res. Letters* **20** (8), 639–641.
- Schmittbuhl, J., Roux, S., Berthaud, Y. (1994). Development of roughness in crack propagation. *Europhysics Letters* **28**, 585–590.
- Schmittbuhl, J., Vilotte, J.-P., Roux, S. (1995a). Reliability of self-affine measurements. *Physics Review E* **51** (1), 131–147.
- Schmittbuhl, J., Schmitt, F., Scholz, C. (1995b). Scaling invariance of crack surfaces. *Geo. Res.* **100**, 5953–5973.
- Schroeder, M., Siegert, M., Wolf, D.E., Shore, J.D., Plischke, M. (1993). Scaling of growing surfaces with large local slopes. *Europhysics Letters* **24** (7), 563–568.
- Simonsen, I., Hansen, A., Nes, O.M. (1998) Using wavelet transformations for Hurst exponent determination. *Physics Review. E* **58** (3), 2779–2787.
- Weiss, J. (2001a). Fracture and fragmentation of ice: a fractal analysis of scale invariance. *Engineering of Fracture and Mechanics* **68**, 1975–2012.
- Weiss, J. (2001b). Self-affinity of fracture surfaces and implications on a possible size effect on fracture energy. *International Journal of Fracture* **109**, 365–381.